This is a pre-print version of the paper: A simulation tool for ion exchange membrane crystallization of magnesium hydroxide from waste brine. Submitted of Journal Chemical Engineering Research and Design

A simulation tool for ion exchange membrane crystallization of magnesium hydroxide from waste brine

F. Vassallo[a], C.Morgante[a], G. Battaglia[a], D. La Corte[a], M. Micari[b], A. Cipollina*[a,c], A. Tamburini[a,c], G. Micale[a,c]

[a] *Dipartimento di Ingegneria, Università degli Studi di Palermo (UNIPA)- viale delle Scienze Ed.6, 90128 Palermo, Italy*

[b] *Institute of Engineering Thermodynamics, DLR, Stuttgart, Germany*

[c] *ResourSEAs SrL, viale delle Scienze Ed. 16, 90128 Palermo, Italy*

*corresponding author: andrea.cipollina@unipa.it

Abstract

Increasing attention is nowadays paid to the management and valorisation of industrial waste brines aiming also at the recovery of raw materials. Magnesium has been listed as a Critical Raw Material by EU, prompting researchers to investigate novel routes for its recovery. Within this framework, a novel Crystallizer with Ion Exchange Membrane (CrIEM), is proposed as an innovative way to recover magnesium from industrial waste brines exploiting low-cost alkaline reactants. In the present work, a novel mathematical model of the CrIEM process is proposed to provide a useful tool for its design in different working conditions. Batch and feed & bleed continuous configurations have been investigated taking into account: (i) the variation of the alkaline and brine concentration in their own collection tanks over time and (ii) the spatial mono-dimensional (1D) steady-state description of the main phenomena that occur inside the CrIEM. Original experimental data, from ad-hoc laboratory tests, and literature information were used to validate the proposed model both in the batch and continuous feed & bleed configuration. A good agreement between model predictions and experimental/literature data was found for both cases, thus proving the reliability of the proposed model for the design of the CrIEM reactor.

Keywords: *circularity, minerals recovery, brine valorisation, membrane crystallizer; ZLD; MLD.*

1 Introduction and literature review

In the last decade, much attention has been paid to the environmental impact of industrial wastes and the availability of raw materials, such as minerals, from conventional sources. Among them, magnesium has been listed as one of the 30 Critical Raw Materials (CRM) by the European Union. [1]. Magnesium has been recently attracting a continuous interest, becoming essential in the framework of the European and global economy, prompting many researchers to investigate novel routes for its recovery. Precisely, more than 1.1 million metric tons were produced worldwide in 2019, a quantity destined to increase according to recent forecasts [2]. However, its exponential rise of importance has led contemporarily to a high risk of supply interruption due to its geopolitical availability [3]. This has urged to seek alternative sources to satisfy the increasing global demand. Therefore, setting aside the conventional methods that have almost reached exhaustion, such as mineral mining [4], more and more interest has been focused on the exploitation of other sources, such as seawater or exhausted industrial brines, which present high concentration in salts and minerals, and especially in magnesium [5]. In fact, the exploitation of unconventional sources and the reuse and valorization of waste streams are key steps towards the change of the industrial economic model, from a linear economy to a circular one.

Seawater represents an unlimited resource of magnesium [6]. More than 70% of the earth surface is covered by water, mainly seawater (more than 90%), and the concentration of magnesium in seawater is between 1.1 and 1.7 kg/m^3 [7]. In addition, magnesium recovery from seawater has shown easier accessibility than those of traditional sources, e.g. mining processes [5].

On the other hand, exhausted brines (originated from saltworks) have a higher magnesium concentration than that of seawater, potentially reaching concentrations up to 30-50 kg/m^3. Moreover, the recovery of magnesium from brines contributes to reduce the environmental impact of these streams [8–10], which are typically discharged into natural water bodies.

In this regard, in the literature, the valorization of exhausted brines to recover magnesium has been widely investigated. In the ‘80s, Al Mutaz [11] analysed the technical feasibility of mineral recovery from exhausted brines discharged from desalination plants focusing on the possibility to recover magnesium [12]. Turek and Gnot [13] tested the possibility to recover magnesium hydroxide as a by-product from a two-stage system (direct mixing step and a sedimentation step) that treated waste brines from chlorine production industry and coal mining brines [14]. In particular, they added sodium hydroxide (NaOH) in order to precipitate magnesium from the brines avoiding the contamination of co-precipitated byproducts. However, the use of NaOH led

to filtration issues that made the sedimentation of magnesium hydroxide ($MgOH_2$) suspension slower and poorly filterable. Sung-Woo and Jun-Heok [15] proposed a multi-step reactive process (based on direct mixing between reactants) to recycle magnesium chloride from waste brines of an industrial membrane based process for the production of NaCl. Authors employed the same alkaline reactant used by Turek (NaOH) to promote the magnesium precipitation. Henrist et al. [16] investigated how alkaline solutions affect the magnesium precipitation in terms of morphology and dimension of crystals via a controlled-double jet precipitation technique. In particular, the authors tested two different alkaline solutions, namely sodium hydroxide (NaOH) and ammonium hydroxide (NH_4OH), observing that cauliflower-shaped globular agglomerates were obtained when NaOH-solution was used as alkaline reactant, whereas, a higher resistant platelet-shaped was obtained with NH_4OH. Overall, many studies have highlighted the possibility to recover magnesium in the form of magnesium hydroxide with high crystals purity by mixing directly exhausted brine with sodium hydroxide solution. Other alkaline compounds, such as calcium hydroxide ($Ca(OH)_2$) or lime (dilute $Ca(OH)_2$ solution), have been found to cause the co-precipitation of by-products (i.e. calcium sulphates, carbonates and hydroxides) reducing the purity of magnesium hydroxide [17]. However, it should be noted that, NaOH solutions are much more expensive than calcium hydroxide or lime ones [18,19].

In this scenario, a novel ion exchange membrane crystallizer (CrIEM) was developed and patented by a research group of the University of Palermo [20,21]. They proposed a novel technology able to recover magnesium in the form of magnesium hydroxide ($Mg(OH)_2$) employing not expensive alkaline solutions, without affecting the final product purity. As a matter of fact, La Corte et al [20] used the CrIEM in a feed & bleed configuration to recover high-purity magnesium hydroxide from real seawater and coal industrial waste brines. To the best of the authors' knowledge, no modelling tools of the CrIEM reactor have been presented in literature yet, despite the benefits that modelling could provide, e.g. identification of the best geometrical configurations and optimal working conditions for such kind of reactor. The present work aims at filling this gap introducing a novel mathematical model of the CrIEM describing the functioning of the reactor in different working conditions. Specifically, batch and feed & bleed configurations have been investigated accounting for the main phenomena characterizing the system. The model was validated through experimental and literature data. An ad-hoc experimental campaign was carried out at the Brine Excellence Center (BEC) of the University of Palermo to collect experimental data of the CrIEM

reactor working in a batch configuration. On the other hand, the experimental results presented by La Corte et al. [20] were adopted for the feed & bleed arrangements.

1.1 The CrIEM reactor

The CrIEM reactor is a membrane-based unit made of two fluid channels separated by an anion exchange membrane (AEM), as depicted in Figure 1.

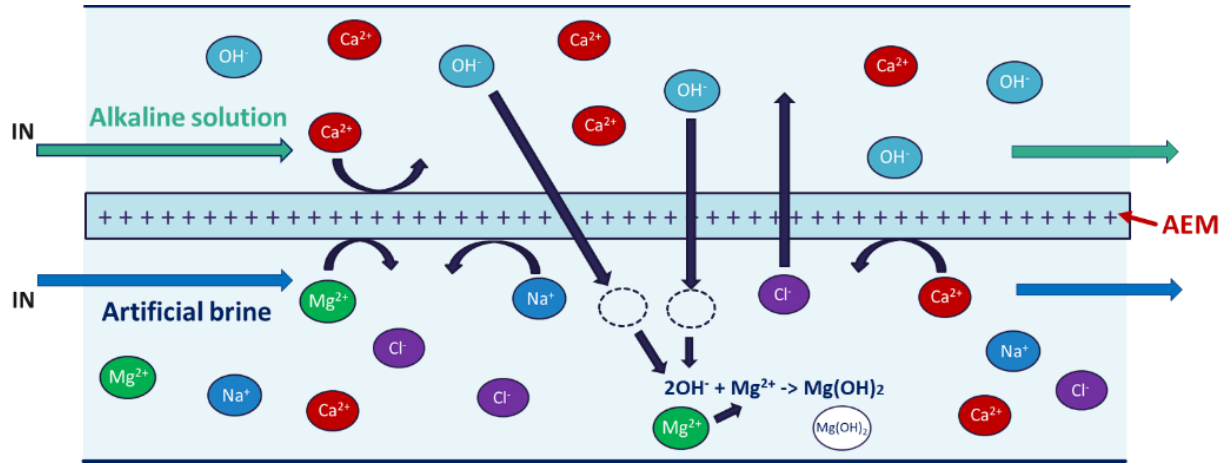

Figure 1: Scheme of the CrIEM reactor

An alkaline solution, $Ca(OH)_2$ solution, and brine, rich in magnesium (Mg^{2+}), are fed into the two separated CrIEM channels. Note that, brines are typically composed of sodium chloride (NaCl), magnesium chloride ($MgCl_2$), and calcium chloride ($CaCl_2$), thus containing a high chlorine ions concentration. The AEM membrane allows the passage of only ions of opposite electric charge with respect to that in the membrane matrix (counter-ions), e.g. hydroxyl (OH^-) and chlorine (Cl^-) ions, from one channel to the other. Conversely, ions of the same electric charge as that of those in the membrane matrix (co-ions) are rejected based on the Donnan Exclusion theory [22]. According to the Donnan theory, the transmembrane fluxes of counter-ions are governed by a double driving force given by a concentration gradient across the membrane and by the generation of an electric potential gradient due to the Donnan equilibrium established at the interfaces of the membrane. Therefore, the induced transmembrane fluxes of OH^- and Cl^- ions, from the alkaline to the brine solution and from the brine to the alkaline solutions, respectively, allows the recovery of magnesium avoiding the direct mixing of the two solutions. As a matter of fact, the hydroxyl ions,

that move from the alkaline solution to the brine, react with magnesium causing the precipitation of magnesium hydroxide, according to the following chemical reaction:

$$Mg^{2+} + 2\,OH^{-} \rightarrow Mg(OH)_2 \downarrow \quad (1)$$

Since magnesium hydroxide has a very low solubility (K_{sp} $5.61 \cdot 10^{-21}$ [mol^3/m^9]), supersaturation is quickly attained reaching a pH value of ~9.8 in the brine solution. At this pH, magnesium ions (Mg^{2+}) instantly react with hydroxide ions, hindering the co-precipitation of other hydroxides. It is worth noting that, while the hydroxyl ions concentration in the alkaline solution decreases as the $Mg(OH)_2$ precipitates, the chlorides ions continuously pass from the brine to the alkaline compartment ensuring a high driving force for the Donnan transport mechanism [20].

2 Experimental set-up and procedures

2.1 Set-up description

To perform the magnesium precipitation in brine solutions adopting a membrane-based reactor unit working in a batch configuration, an experimental set-up made by the CrIEM reactor and two external tanks was used. The developed experimental set-up is shown in Figure 2a. Specifically, the CrIEM module has a plate and frame layout, consisting of two Plexiglas plates 180 mm long, 260 mm wide and 23 mm thick equipped with an AEM E1 type 10 anion exchange membrane (Fujifilm B.V. Europe, see Table 1). In each plate, a semi-circular zig-zag shaped channel is excavated with a diameter of 8.14 mm and a total length of 1800 mm, as can be seen in Figure 2b. Both channels present two circular holes at their ends in which locking fittings are mounted to connect the module to the two external tanks by means of a hydraulic circuit. In particular, semi-rigid PE (polyethylene) pipes of inner diameter of 6 mm, are used to guarantee adequate chemical resistance to the very corrosive employed chemical compounds. During the experimental run, pressure drops within the reactor are monitored in order to avoid any damage/rupture of the membrane caused by blocking of the channels. Therefore, two pressure gauges are placed at both inlets of the reactor. As stated above, the CrIEM reactor is connected to the two external tanks by means of PE pipes. One tank contains the brine, while the other contains the alkaline solution. A perfect mixing condition of the solutions is guaranteed by employing a magnetic stirring bar introduced in each tank. Both solutions (the brine solution and the alkaline one) are circulated into

the system using two peristaltic pumps (SEKO, mod. Kronos 50, and Lead Fluid, model WT/600/S), thus accomplishing a batch operating mode. In addition, a pH meter (Hanna, Series HI5000) is employed to monitor the pH of the brine throughout the experimental tests.

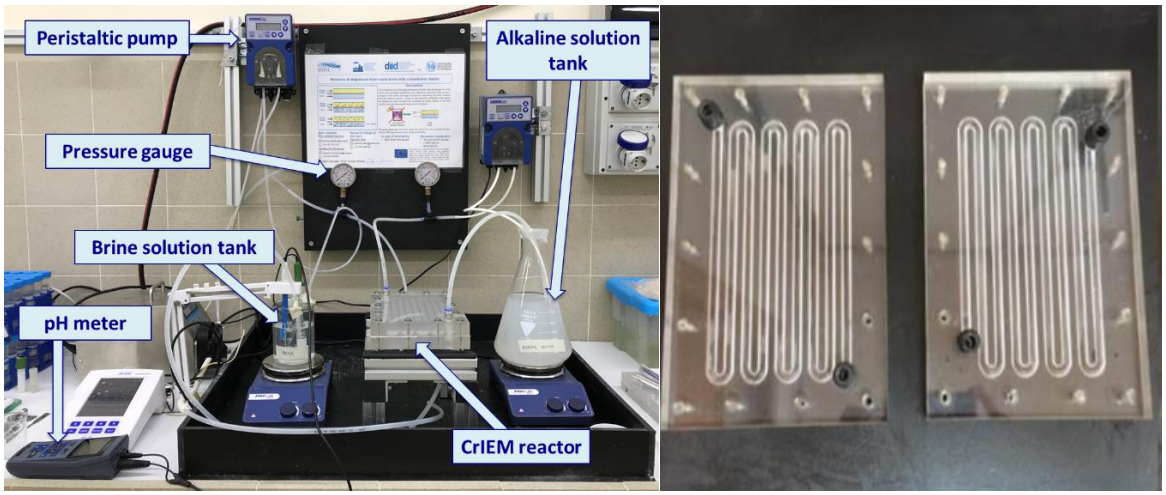

Figure 2.a) Experimental set-up of the CrIEM reactor. b) An insight of the channel excavated in the CrIEM plates.

Table 1.Properties of the Fujifilm AEM membrane E1 type 10 [23].

Item		Specification
Selectivity	%	95-98
Water Permeability	gr/hr/bar/m^2	8
Charge Density	mol/kg	2.85
Stability	pH	1-13
Thickness (dry)	µm	120

Membrane was conditioned in an aqueous solution of sodium chloride (NaCl) at a concentration about 0.6 M for, at least, 12 hours before conducting any experiment.

2.2 Experimental procedure

The employed brine and the alkaline solutions were prepared starting from deionized water generated by two steps of reverse osmosis (conductivity below 0.5 µS/cm). Calcium hydroxide ($Ca(OH)_2$) pellets (purity > 96%, Sigma Aldrich, USA) were used to prepare supersaturated alkaline suspensions (10% more concentrated with respect to their stoichiometric value). Furthermore, the alkaline tank was filled with a 3 L of $Ca(OH)_2$ solution in order to avoid an

excessive chloride concentration during the whole experiment run guaranteeing a high driving force of the process.

Brine solutions were made by dissolving salts in deionized water. Salts used to make the brine solution are: magnesium chloride hexahydrate ($MgCl_2 \times 6H_2O$) (purity > 99%, Chem-Lab, Belgium), calcium chloride dehydrate ($CaCl_2 \times 2H_2O$) (purity >99%, Honeywell, Germany) and sodium chloride (NaCl) (purity > 99.5%, Saline di Volterra, Italy). Table 2 lists the brine and alkaline solutions prepared for each experimental test. The final composition of all the solutions were checked via ion chromatography.

Throughout the experimental run, the CrIEM reactor was placed in a horizontal manner, as can be seen in Figure 1a, thus the two fluid channels were one below and one above the AEM membrane. This arrangement ensured a reduction of membrane fouling due to the precipitation of the crystals on the membrane surface, which could cause a considerable reduction of the transmembrane ionic flux. The brine solution was pumped in the channel below the membrane, while the alkaline solution into the above one. As a consequence, the precipitated $Mg(OH)_2$ particles settled in the brine channel towards the channel plexiglass surface rather than the membrane one. After the module assembly, a leakage test was performed. To this end, deionized water was pumped for approximately 30 minutes in one channel of the two, while, in the adjacent channel, air was sent in order to detect any internal or external leakages. Once the system was checked, the CrIEM reactor was connected to the two external tanks and the test started.

To study the behavior and the feasibility of magnesium recovery using the CrIEM in a batch configuration, two tests were performed. For each test a different composition of brine was studied at three different velocities, details are reported in Table 2. The minimum flow rate was 200 ml/min in order to guarantee the circulation of cleaning balls inside the brine channel, used to hinder the formation of scaling on the membrane surface during the experimental run. Each test was run three times for reproducibility purpose.

Table 2.Initial composition of the main ions of the brine and alkaline solution and operative conditions adopted in the experimental tests.

		Ions concentration in the Brine solution [g/l]				Concentration in the alkaline suspension [g/l]	Flow-Rate [ml/min]		Initial Volume [l]	
Tests		Na^+	Ca^{2+}	Mg^{2+}	Cl^-	$Ca(OH)_2$	Brine	Alkaline	Brine	Alkaline
1	Case #1	8.5	0.4	1.14	17.1	1.88	300	160	0.5	2
	Case #2	8.16	0.39	1.12	16.5		250			
	Case #3	8.10	0.39	1.10	16.4		200			
2	Case #1	7.87	0.36	2.04	18.7	3.35	300	160	0.5	3
	Case #2	7.84	0.33	2.00	18.5		250			
	Case #3	7.69	0.34	1.98	18.2		200			

The experimental tests ended once all magnesium ions, in the brine solution, were converted into magnesium hydroxide ($Mg(OH)_2$). An estimation of the conversion degree during the experimental test was done by monitoring the pH of the brine. Specifically, the OH- flux from the alkaline to the brine solution causes an increase of the brine pH until a value of ~ 9.8. Above this value, the precipitation of $Mg(OH)_2$ begins. When the amount of Mg ions is significantly consumed, pH starts slightly increasing up to around 10.35, when all Mg ions have reacted and the pH trend sharply increases [20]. Note that, pH higher than 10.35 indicates that all Mg ions are converted. This pH represents the equilibrium condition of the magnesium hydroxide precipitation process (as can be estimated by taking into account the magnesium hydroxide solubility product, i.e. 5.61×10^{-12} at 25°C [24]).

2.3 Sampling and analytical procedures

The *produced slurry*, i.e. the suspension of $Mg(OH)_2$, was sampled at regular time intervals throughout the experiments. The sampling interval was chosen differently for each set of tests as the total conversion of magnesium was accomplished at significantly different experimental times due to the different magnesium concentration in the two investigated brines, i.e. Mg ions in the brine of Test 2 was almost the double of that in Test 1. For the first set of tests, a sampling interval of 40 minutes was chosen. Conversely, for the second set, a sampling interval equal to 60 minutes was adopted. For each sample, a volume of 50 ml of suspension was withdrawn from the brine tank. A small amount of the suspension was filtered by using a micro-filter (0.45 μm filter) in order to separate the solids from the solution. The filtered solution was then analysed by performing a chromatographic analysis (Ionic Chromatographic Metrohm 882 Compact IC plus) to determine

the cationic composition of the filtered solution. In order to prepare the samples for the chromatographic analysis, the filtered solution was first diluted at 1:100 using deionised water and again filtered via the same micro-filter.

Once the magnesium composition was detected, the conversion of magnesium in magnesium hydroxide over the experimental time was computed by using the following equation:

$$Conversion = \frac{C_{Mg^{2+}} \cdot V_{brine}|_{t=0} - C_{Mg^{2+}} \cdot V_{brine}|_{t}}{C_{Mg^{2+}} \cdot V_{brine}|_{t=0}} \quad (2)$$

where, $C_{\mathrm{Mg^{2+}}}$ is the concentration of magnesium inside the brine tank, V_{brine} is the volume of the brine solution and the subscript *t* refers to the time of the sampling.

3 Modelling

In this section the mathematical description of the functioning of a CrIEM system is addressed mainly considering a batch configuration. Few adjustments are also discussed in order to extend the model for the analysis of feed & bleed arrangements.

3.1 Modelling of the CrIEM reactor in a batch configuration

Spatial and time differential mass balances and phenomenological transport equations were taken into account to investigate the performance of a CrIEM reactor in a batch configuration. In the model, the phenomena occurring inside the reactor were described assuming a steady-state regime, thus considering only a spatial variation of the ion concentrations and the flow rates along the channel length. Conversely, a time-dependent approach was adopted to depict the phenomena occurring in the two tanks.

3.1.1 Mass balances and mass transport in the CrIEM channels

A one-dimensional (1-D) finite difference discretization approach was used to address the differential mass balance equations in the CrIEM along the channel length. Mass balance equations were solved assuming negligible axial and radial diffusion and taking into account an instantaneous precipitation of magnesium hydroxide crystals in the brine channel. This latter assumption is well justified by the fact that the precipitation of $Mg(OH)_2$ is a very fast process [3].

Figure 3 presents a schematic representation of the one-dimensional computational domain adopted in the study of the CrIEM channels.

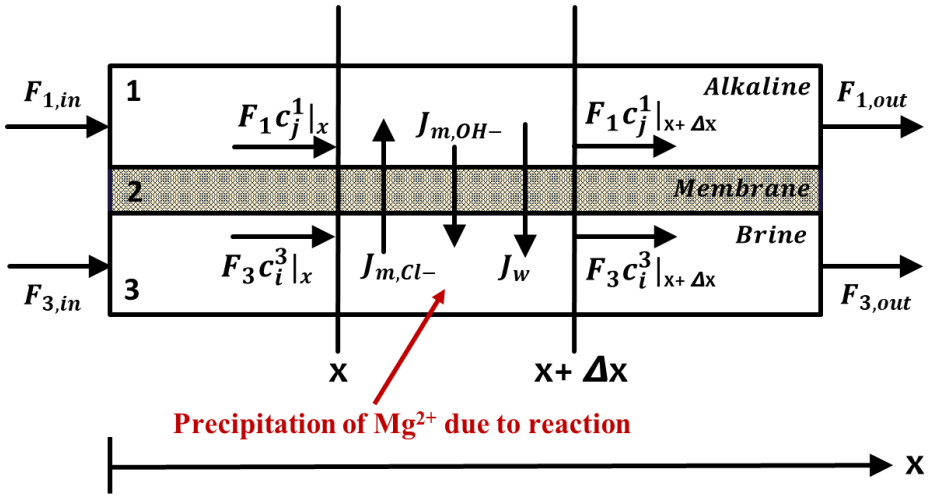

Figure 3: Schematic representation of the discretized domain of the CriEM channels: main quantities, flow channels (1 alkaline, 3 brine) and the membrane (2 AEM).

As can be seen in *Figure 3*, the alkaline and brine solutions are assumed to flow in the same direction, referring to a co-current configuration. Under this assumption, differential mass balance equations were written for the two solutions as:

$$\frac{dF_1}{dx} = -J_w W \tag{3}$$

$$\frac{dF_3}{dx} = J_w W \tag{4}$$

$$\frac{dc_j^1 F_1}{dx} = \pm J_{m,j} W \tag{5}$$

$$\frac{dc_i^3 F_3}{dx} = \pm J_{m,i} W \tag{6}$$

where F_1 and F_3 are the flow rate of the alkaline and brine solutions [m^3/s], respectively; J_w is the water flux through the membrane [m^3/m^2s]; W is the channel width [m]; c_j^1 and c_i^3 are the concentration of the j^{th} and i^{th} species in the alkaline and brine solution [mol/m^3], respectively. The subscript j refers to Ca^{2+}, Cl^- and OH^- ions present in the alkaline solution, while the subscript i refers to Mg^{2+}, Ca^{2+}, Na^+, Cl^- and OH^- ions of the brine solution. $J_{m,j}$ and $J_{m,i}$ are the fluxes of the species j and i through the membrane [mol/m^2s]. It is worth noting that, only anionic species were assumed to pass across the membrane, while the passage of all the cationic species is forbidden (total rejection of the membrane).

To consider the magnesium hydroxide precipitation in the brine channel, it was assumed that the hydroxyl ions entering the brine channel through the membrane instantaneously react with magnesium ions. Therefore, the i^{th} Eq. (6) referred to magnesium ions was modified as:

$$\frac{dc^3_{Mg^{2+}}F_3}{dx} = -\frac{J_{m,OH^-}W}{2} \tag{7}$$

In regard to the alkaline channel, the dissolution of calcium hydroxide particles was also taken into account. As explained in Section 2, experimental tests were run using a supersaturated calcium hydroxide solution in order to ensure an almost constant OH^- concentration throughout the experimental runs (balancing the OH^- ions leaving the channel through the membrane). Therefore, the dissolution equilibrium condition of the $Ca(OH)_2$ through its K_{ps} (i.e. 5.5×10^{-15} [mol^3/m^9] [25]) was considered:

$$K_{ps} = c^1_{Ca^{2+}}(c^1_{OH^-})^2 = 5.5 \times 10^{-15} \tag{8}$$

However, solution's electroneutrality has to be always satisfied in the channel:

$$z_{Ca^{2+}}c^1_{Ca^{2+}} = z_{OH^-}c^1_{OH^-} + z_{Cl^-}c^1_{Cl^-} \tag{9}$$

where $z_{Ca^{2+}}$, $z_{OH^-}$and z_{Cl^-} are the chemical valence of calcium, hydroxyl and chloride ions, respectively. Eqs. (8) and (9) allow the accurate estimation of the calcium ions concentration in the alkaline channel.

Membrane-based separation processes are typically affected by concentration polarization phenomena, which are caused by the different kinetics of ion transport in solutions and in membranes [26]. Concentration polarization phenomena lead to concentration gradients between membrane interface and bulk solution, reducing, in turn, the transmembrane fluxes. In the present model, however, such phenomena were neglected for the sake of simplicity. Therefore, concentration ions at the solutions bulk and at the membrane interfaces were assumed to be the same:

$$c^{1\ or\ 3,bulk}_{i\ (or\ j)} = c^{1\ or\ 3,w}_{i\ (or j)} \tag{10}$$

where $c^{1\ or\ 3,bulk}_{i\ (or j)}$ is the bulk concentration in the alkaline (1) or the brine (3) channel, while $c^{1\ or\ 3,w}_{i\ (or j)}$ is the concentration at the membrane-solution interface.

In addition, the electroneutrality condition has to always be satisfied both at the solutions bulk and at the membrane-solution interfaces:

$$\sum_{i\ (or\ j)}^{p\ (or\ q)} \left(z_{i\ (or\ j)} c_{i\ (or\ j)}^{1\ or\ 3,bulk}\right) = 0 \tag{11.a}$$

$$\sum_{i\ (or\ j)}^{p\ (or\ q)} \left(z_{i(or\ j)} c_{i\ (or\ j)}^{1\ or\ 3,w}\right) = 0 \tag{11.b}$$

where p and q are the total number of ionic species present in the alkaline and the brine solution, respectively.

3.1.2 Mass transport and Equilibrium phenomena in the membrane

An anion exchange membrane (AEM) presents positively charged ions in its own polymeric matrix, which are typically called fixed charges [27]. The presence of fixed charges allows a selective passage of ions from a solution to another one. Ideally only ions can pass across the membranes, however a non-ideal water flux always occurs in real applications. Therefore, in the case of the CrIEM reactor, anionic ions, namely hydroxyl and chloride, and water fluxes have to be taken into account to describe the variation of ions concentration across the membrane and along the channels length. In this regard, the CrIEM reactor can be studied as a dialyzer based on the Donnan Dialysis principles. Furthermore, hydroxyl and chloride ions fluxes through the membrane can be calculated employing the Nernst-Plank equation [28]:

$$J_{m,k} = -D_{m,k} \frac{\Delta c_k^m}{\delta} - \frac{D_{m,k} z_k \bar{c}_k^m F \Delta\Psi}{RT\delta} \tag{12}$$

In Eq. (12), the ionic transmembrane flux ($J_{m,k}$) of the *k* species, i.e. OH^- or Cl^-, is given by the sum of a diffusion flux (first element on the right part of the equation) and a migrative flux (second element on the right part of the equation), while the convective contribution is here neglected since no convection occurs within the membrane matrix [29]. $D_{m,k}$ is the diffusion coefficient [m^2/s]. Δc_k^m is the concentration gradient within the membrane between its two surfaces [mol/m^3]. δ is the width of the membrane [m], z_k is the chemical species valence, $\bar{c}_k^m$ is the average concentration in the membrane [mol/m^3], F is the Faraday constant [C/mol], R is the universal gas constant

[J/mol K], T is the absolute temperature [K] and $\Delta\Psi$ is the electric potential gradient within the membrane [V].

As far as the diffusion coefficients of hydroxyl and chloride ions in the membrane are concerned, they vary in a wide range depending on membrane properties and operative conditions: D_{OH^-} = $8.6\times10^{-12} \div 8.7\times10^{-11}$ and D_{Cl^-} = $4\times10^{-12} \div 1.5\times10^{-10}$ m^2/s [30]. Within these ranges, D_{OH^-} = 2.2×10^{-11} m^2/s and D_{Cl^-} = 3.4×10^{-11} m^2/s were employed in the model. Note that experimental data were well fitted by model predictions adopting these values.

In Donnan Dialysis no external electric potential is applied, implicating that no net electric current passes through the membrane. Therefore, the sum of ionic transmembrane fluxes has to be null [31]:

$$J_{m,OH^-} + J_{m,Cl^-} = 0 \tag{13}$$

Substituting Eq. (12) into Eq. (13), the electric potential gradient $\Delta\Psi$ can be expressed as:

$$\Delta\Psi = \frac{RT}{F}\frac{(D_{m,OH^-}\times\Delta c^m_{OH^-} + D_{m,Cl^-}\times\Delta c^m_{Cl^-})}{(-z_{Cl^-}\times D_{m,Cl^-}\times\bar{c}^m_{Cl^-} - z_{OH^-}\times D_{m,OH^-}\times\bar{c}^m_{OH^-})} = \frac{RT}{F}(\alpha_1+\alpha_2) \tag{14.a}$$

$$\alpha_1 = \frac{D_{m,OH^-}\times\Delta c^m_{OH^-}}{(-z_{Cl^-}\times D_{m,Cl^-}\times\bar{c}^m_{Cl^-} - z_{OH^-}\times D_{m,OH^-}\times\bar{c}^m_{OH^-})} \tag{14.b}$$

$$\alpha_2 = \frac{+D_{m,Cl^-}\times\Delta c^m_{Cl^-}}{(-z_{Cl^-}\times D_{m,Cl^-}\times\bar{c}^m_{Cl^-} - z_{OH^-}\times D_{m,OH^-}\times\bar{c}^m_{OH^-})} \tag{14.c}$$

In the model, Donnan equilibria at membrane-solution interfaces were also considered in order to compute the hydroxyl ion concentrations at the membrane surface (membrane side) [32]:

$$c^{1\ or\ 3,m}_{OH^-} = \frac{c^{1\ or\ 3,w}_{OH^-}\, c^{1\ or\ 3,m}_{Cl^-}}{c^{1\ or\ 3,w}_{Cl^-}} \tag{15}$$

where superscripts 1 and 3 refer to the alkaline and the brine channel, while m and w refer to the concentration of hydroxyl or chloride ions inside the membrane and at the solutions-membrane interfaces, respectively. Furthermore, the corresponding chloride ion concentrations were calculated taking into account the electroneutrality condition:

$$c_{Cl^-}^m = X_+^m - c_{OH^-}^m \quad (16)$$

where X_+^m is the concentration of the fixed charges in the membrane matrix.

Concerning water flux through the membranes, it is made of two main contributions, *i.e.* osmotic and the electro-osmotic flux [33]:

$$J_w = P_{os}\Delta\pi + \sum_k \beta_k J_{m,k} \quad (17)$$

where P_{os} is the water permeability of the membrane [m^3/(Pa m^2 s)], $\Delta\pi$ is the difference of osmotic pressure between the two channels [Pa] and β_k refers to the hydration number of the hydroxyl and chloride ions, i.e. 6 and 7, respectively [34]. The osmotic pressure was calculated using the van't'Hoff equation in which osmotic coefficients were considered to be unitary.

3.1.3 Mass balances in the tanks

As described in Section 2, the CrIEM reactor is connected to two tanks containing the alkaline and brine solutions. Figure 4 illustrates a conceptual design of the experimental set-up of Section 2 reporting the nomenclature of solution flow rates and ion concentrations adopted in the present model.

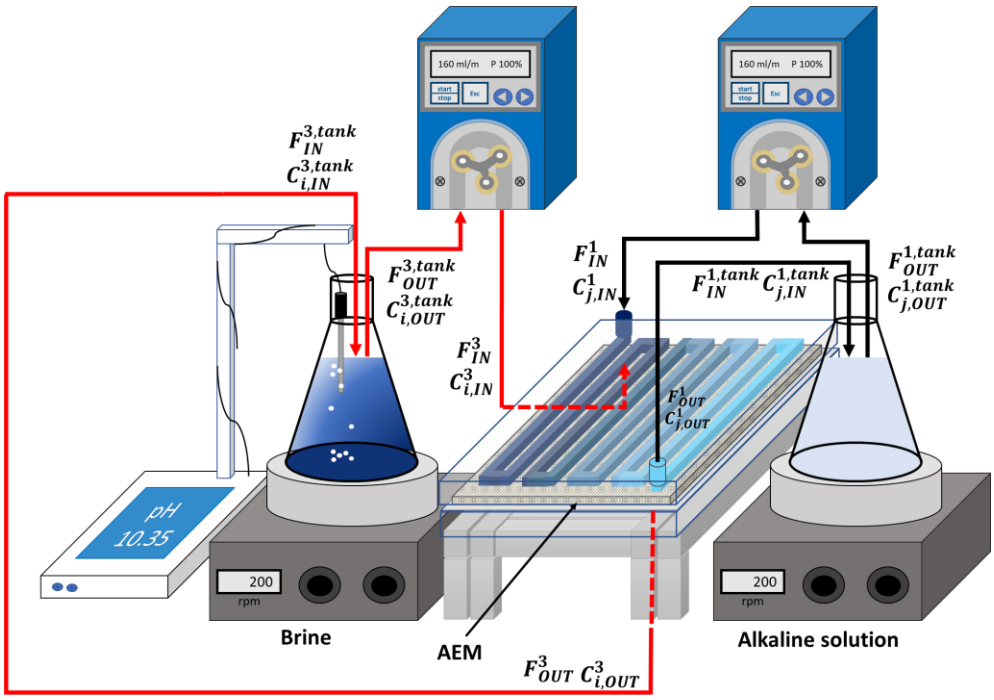

Figure 4.Conceptual design of the experimental set-up of the CrIEM reactor.

Solution concentrations and volumes variation over time in the two tanks can be investigated considering time differential mass balance equations:

$$\frac{d\rho^{1,tank}V^{1,tank}}{dt} = \rho_{IN}^{1,tank}F_{IN}^{1,tank} - \rho_{OUT}^{1,tank}F_{OUT}^{1,tank} \quad (18)$$

$$\frac{d\rho^{3,tank}V^{3,tank}}{dt} = \rho_{IN}^{3,tank}F_{IN}^{3,tank} - \rho_{OUT}^{3,tank}F_{OUT}^{3,tank} \quad (19)$$

$$\frac{dc_j^{1,tank}F^{1,tank}}{dt} = c_{j,IN}^{1,tank}F_{IN}^{1,tank} - c_{j,OUT}^{1,tank}F_{OUT}^{1,tank} \quad (20)$$

$$\frac{dc_i^{3,tank}F^{3,tank}}{dt} = c_{i,IN}^{3,tank}F_{IN}^{3,tank} - c_{i,OUT}^{3,tank}F_{OUT}^{3,tank} \quad (21)$$

where $\rho^{1,tank}$, $V^{1,tank}$ and $F^{1,tank}$ are the density [kg/m^3], the volume [m^3] and the flow rate [m^3/s] of the alkaline solution, while $\rho^{3,tank}$, $V^{3,tank}$ and $F^{3,tank}$ are referred to the brine. $c_j^{1,tank}$is the concentration of the j^{th} species in the alkaline solution [mol/m^3], i.e. Ca^{2+}, Cl^-, OH^-. $c_i^{3,tank}$is the concentration of the i^{th} species in the brine solution [mol/m^3], i.e. Mg^{2+}, Ca^{2+}, Na^+, Cl^-, OH^-. Subscripts IN or OUT refer either to flow rates or concentrations that enter or exit their respective tanks.

Solutions were considered perfectly mixed at each instant of the process and their density was computed implementing a dedicated algorithm developed for aqueous multicomponent electrolyte solutions [35].

Mass balances in the two tanks, Eqs. (18)-(21), were solved adopting a finite difference scheme and a time discretization interval equal to the residence time in the CrIEM channels. Magnesium ions conversion in the brine was also assessed using Eq. (2).

3.1.4 Numerical algorithm for batch configuration

Spatial discrete mass balance equations of the CrIEM reactor, Eqs. (3)-(6), and time discrete mass balance equations of the two tanks, Eqs. (18)-(21), have to be solved contemporarily along with mass transport, Eqs. (12)-(13)-(14.a)-(17), and phenomenological equations, Eqs. (15)-(16), to determine the performance of a CrIEM reactor in a batch configuration. To this aim, an original algorithm was developed and implemented in Python. A closure assumption was made to couple Eqs. (3)-(6) and Eqs. (18)-(21). Specifically, flow rates and ion compositions of the solutions entering the CrIEM were assumed to be equal to those exiting the two tanks, thus neglecting any phenomena occurring in the hydraulic system. Similarly, solutions exiting the CrIEM had the same flow rates and ionic composition of those entering the tanks.

The developed algorithm can be divided into three main steps.

1. The first step (green boxes) is based on an iterative procedure performed at each discretized Δx length of the CrIEM channels. Starting from the first discretized element, bulk solution hydroxyl and chloride concentrations are given as initial values at both membrane surfaces, i.e. $c_{Cl^-}^{1,m}$, $c_{Cl^-}^{3,m}$, $c_{OH^-}^{1,m}$ and $c_{OH^-}^{3,m}$. Then, Donnan equilibria (Eq. 15) and the electroneutrality condition in the membrane (Eq. 16) are used to compute new concentrations values. Subsequently, the absolute difference (ε) between the hydroxyl or chloride concentration values of two consecutive iterations is calculated at each membrane interface $\left(\varepsilon = \left| c_{OH^-(or\ Cl^-)}^{1\ (or\ 3),m,NEW} - c_{OH\ (or\ Cl^-)}^{1\ (or\ 3),m,OLD} \right|\right)$. Membrane concentrations are found when all ε become lower than 10^{-5}.
2. The following second step (red boxes) consists in the calculation of the electric potential gradient and the two anionic fluxes in the membrane using Eq. (14.a) and Eq. (12) at each discretized Δx length of the CrIEM. Then, the water flux through the membrane is

computed using the Eq. (17). Finally, the flow rates and ionic concentrations exiting the discretized Δx in both channels are obtained using Eqs. (3-7). The procedure of both Step I and Step II are then performed for the next discretized Δx until the total channel length is covered.

3. Once the CrIEM outlet flow-rates and ion concentrations are calculated from Step I, the third step (blue boxes) allows to apply the mass balance equations (Eqs. 18-21) in the two tanks to compute the volume variation and ion concentrations inside each tank. In addition, magnesium conversion is estimated using Eq. (2).

The whole algorithm terminates when the conversion of the magnesium in the brine tank reaches the desired value. Otherwise, computed new concentration values of Step III are inputted as inlet values in Step I. A flow diagram of the developed algorithm is illustrated in Figure 5.

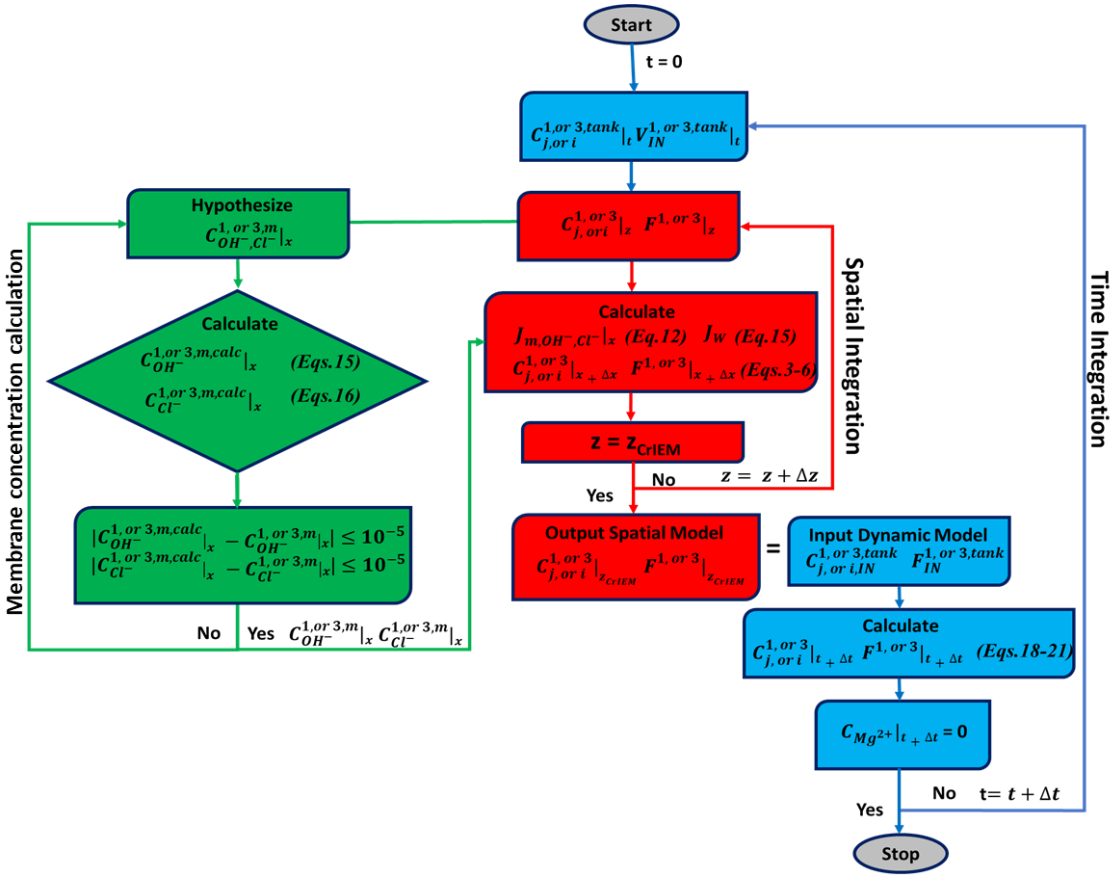

Figure 5. Flow diagram of the developed algorithm for the numerical resolution of the CrIEM model in batch configuration.

3.1.5 Grid size sensitivity analysis

A grid-size analysis was carried out to examine the sensibility of the model predictions on grid resolution. Five grid sizes (Δx) were considered: 0.9 m, 0.45 m, 0.2 m, 0.1 m and 0.05 m. The magnesium concentration profile along the brine channel computed for all the five grid sizes is reported in Figure 6.

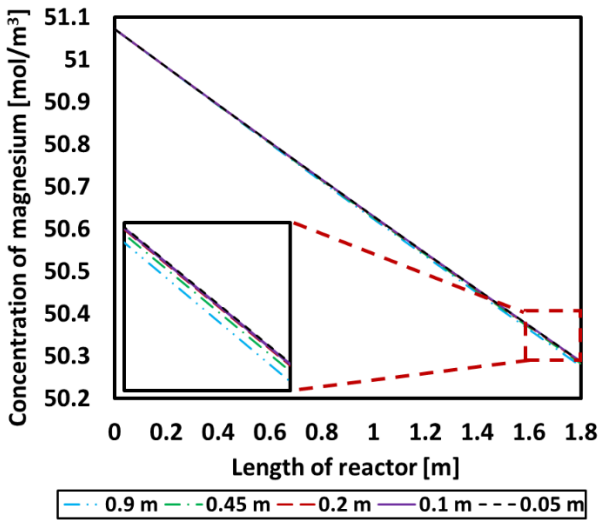

Figure 6. Magnesium concentration profiles along the brine channel length computed using different discretization sizes: 0.9 m, 0.45 m, 0.2 m, 0.1 m and 0.05 m.

As can be seen in Figure 6, a length discretization Δx equal to 0.1 m (solid purple line) can be deemed to satisfy the trade-off between computational effort and model accuracy. This discretization value was used for all the model results presented hereinafter.

3.2 Modelling of the CrIEM reactor in a Feed and bleed configuration

The mathematical model developed in section 3.1 was also appropriately adjusted in order to simulate a CrIEM system working in a feed & bleed configuration. A feed & bleed process consists of two steps: (i) a start-up batch step and (ii) a continuous feed & bleed one. In the first step, all the magnesium ions of the brine solution contained in a buffer tank are converted in $Mg(OH)_2$ particles adopting a batch process, as discussed in Section 2. In the second step, fresh brine (the

feed) is fed into the buffer tank, while the produced suspension (the bleed) is withdrawn from the bottom of the same tank [20]. The feed flow rate is chosen in order that all the magnesium ions added in the buffer tank are converted in a one-through CrIEM passage. A conceptual scheme of this arrangement is shown in Figure 7.

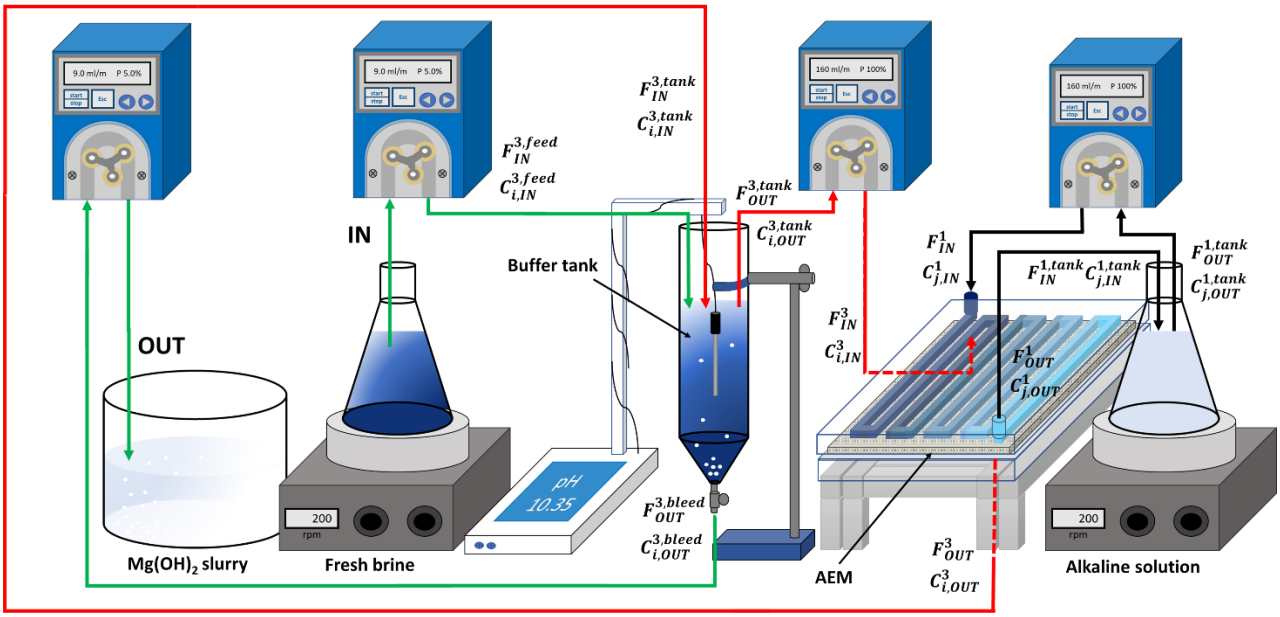

Figure 7.Conceptual design of the CrIEM reactor in a feed and bleed configuration.

To model the feed & bleed configuration two additional terms were added into Eqs. (19) and (21) to consider (i) the addition of fresh brine in the buffer tank and (ii) the withdrawal of the produced suspension:

$$\frac{d\rho^{3,tank}V^{3,tank}}{dt} = \rho_{IN}^{3,tank}F_{IN}^{3,tank} - \rho_{OUT}^{3,tank}F_{OUT}^{3,tank} + \rho_{IN}^{3,feed}F_{IN}^{3,feed} - \rho_{OUT}^{3,feed}F_{OUT}^{3,bleed} \quad (22)$$

$$\frac{dc_i^{3,tank}V^{3,tank}}{dt} = c_{i,IN}^{3,tank}F_{IN}^{3,tank} - c_{i,OUT}^{3,tank}F_{OUT}^{3,tank} + C_{i,IN}^{3,feed}F_{IN}^{3,feed} - C_{i,OUT}^{3,bleed}F_{OUT}^{3,bleed} \quad (23)$$

where, $F_{IN}^{3,feed}$, $\rho_{IN}^{3,feed}$, $C_{i,IN}^{3,feed}$ are the flow rate, the density and the concentration of the fresh brine fed to the buffer tank, while $F_{OUT}^{3,bleed}$, $\rho_{OUT}^{3,feed}$ and $C_{i,OUT}^{3,bleed}$ are the flow rate, the density and the concentration of the slurry withdrawn from the bottom of the buffer tank.

The CrIEM reactor was initially simulated in batch mode. Once a desired magnesium conversion in the buffer tank is achieved, Eqs. (19) and (21) were substituted by Eqs. (22) and (23), thus simulating the continuous feed and bleed step.

3.2.1 Numerical algorithm for Feed & bleed configuration

The CriEM resolution algorithm in a feed & bleed configuration presents several differences in its structure to the one in a batch mode. As depicted in Figure 8, it is possible to observe that the equations employed for the spatial integration of the chemical-physical phenomena within the reactor remain the same as those reported in paragraph 3.1.4. As already mentioned previously, until the concentration of magnesium (present in the brine tank) is lower than a desired value, the CrIEM reactor operates in batch mode. However, as soon as the latter value reaches or exceeds a desired one, the feed & bleed option is activated. From this moment onwards, within the time integration loop, the feed & bleed option is always activated bypassing Eqs. (18)-(21) and computing outlet flow rates and concentrations via Eqs. (22)-(23). The simulation run is brought to an end when the time computed reaches a final given value.

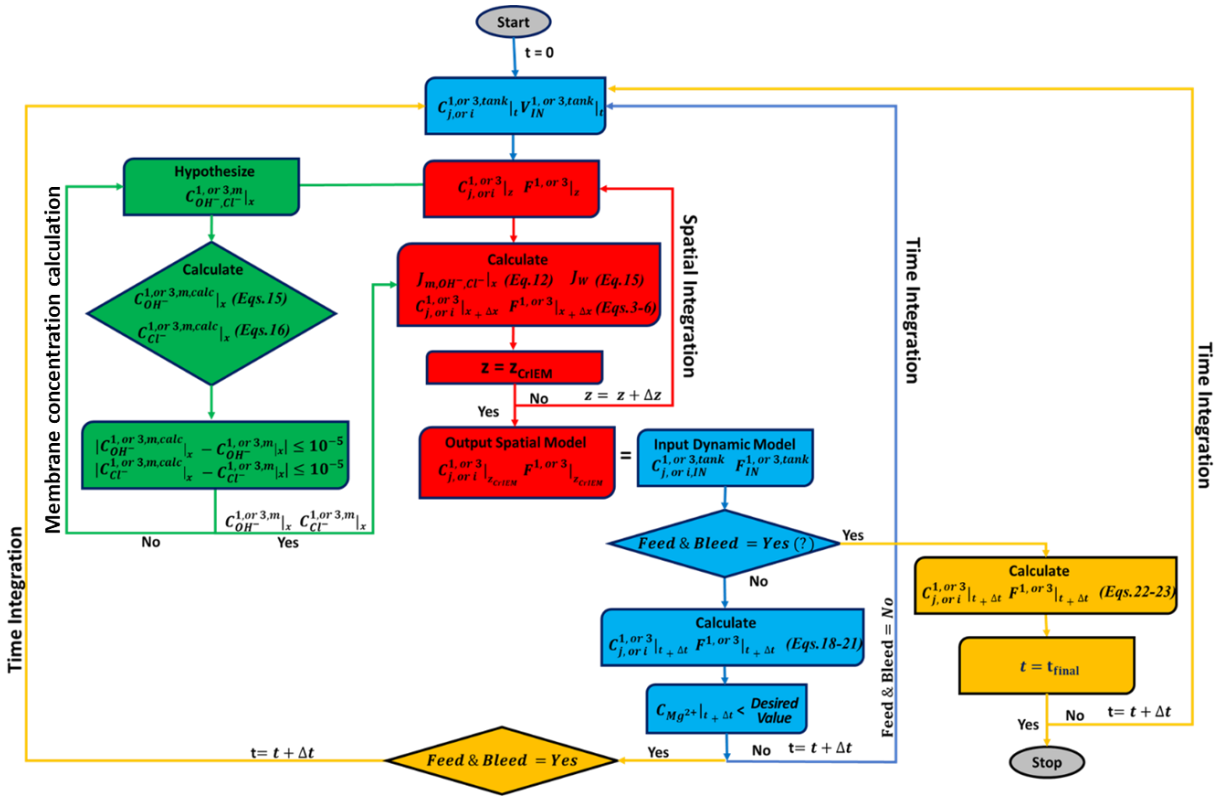

Figure 8: Flow diagram of the developed algorithm for the numerical resolution of the CrIEM model in a feed & bleed configuration.

4 Results and Discussion

In this section model predictions are reported for the case of the CrIEM reactor in batch configuration as described in Section 2 and compared with experimental results so far collected in order to fully validate the simulation tool. Model predictions are also reported for a feed & bleed application and compared with available literature data. Results are discussed in order to show the reliability of the developed model at simulating CrIEM systems.

4.1 Batch configuration

The trend of magnesium conversion over time predicted by the model for all cases of test 1 (see Table 2) is shown in Figure 9. It is possible to observe that the brine flow rate has a negligible influence on the trend of magnesium conversion, as values overlap for all the three investigated flow rates, namely 200, 250 and 300 ml/min. This is due to the high brine flow rates (equal or higher than 160 ml/min). Note that, high flow rates are taken into consideration for several reasons: (i) to hinder possible experimental scaling phenomena (that is not considered in the model) and (ii) reduce concentration polarization in the channels. Figure 9 also reports magnesium conversions experimentally measured. A very good agreement is found between model and experimental results with discrepancies lower than 10% in all cases.

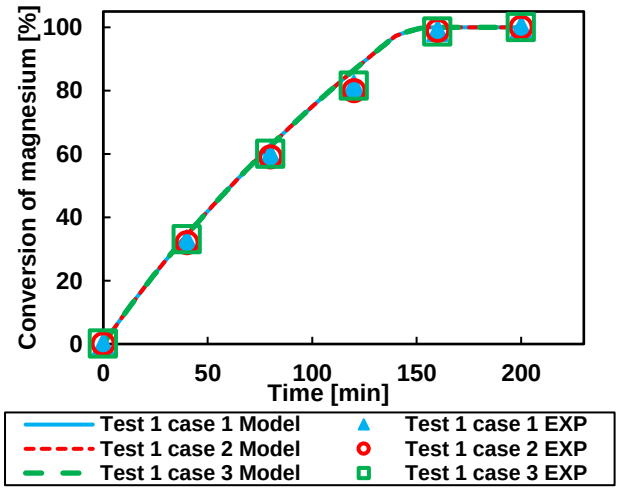

Figure 9. Magnesium conversion over time for Test 1: experimental results and model predictions for case 1 (blue hollow triangle; blue dotted line), case 2 (red hollow circle; red course dashed line) and case 3 (green hollow square; green fine dashed line).

Figure 10 presents further comparisons between model predictions and experimental results considering both Test 1 and Test 2 (Table 2).

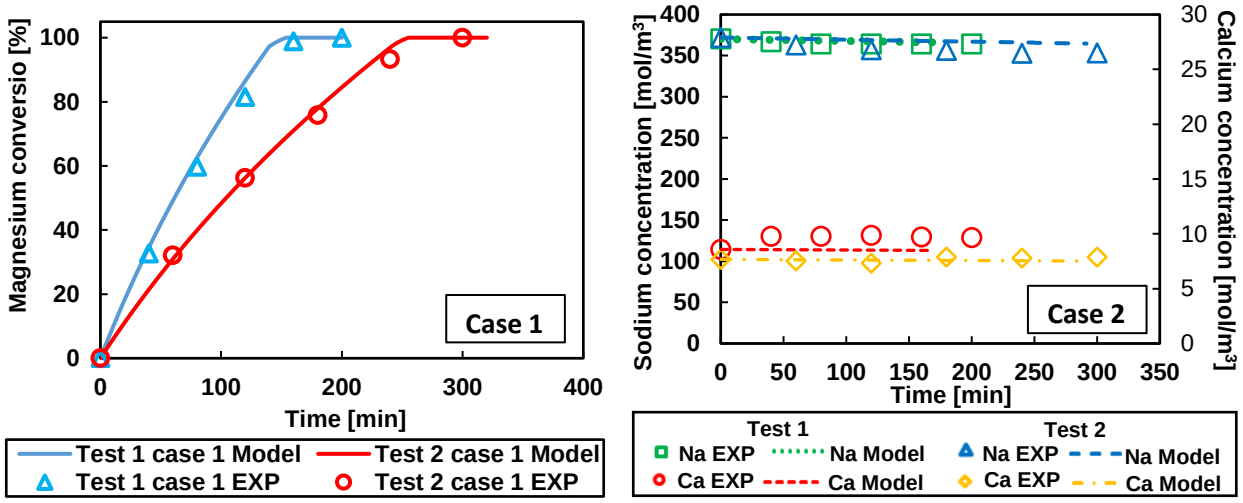

a) **b)**

Figure 10. Magnesium conversion (a), calcium and sodium ion concentration (b) profiles for cases 1 of Tests 1 and 2. Lines and symbols refer to model and experimental results, respectively.

Figure 10-a shows the influence of the initial concentration of magnesium ions on the time required to accomplish their complete conversion. As can be expected, the higher the initial concentration, the higher the conversion time. A conversion time of ~300 min was detected for case 1 of Test 2, while a ~1.5 times lower conversion time characterized Test 1 (~200 min). Results also show that the slope of the magnesium conversion trend gradually decreases over time due to the continuous reduction of the magnesium concentration in the brine. The developed model well predicts the observed experimental trends in all cases (see lines in Figure 10-a). The biggest discrepancy was found to be ~17% for case 1 of Test 2 at an experimental time of 60 min, while all the other discrepancy values were lower than 5%.

To further investigate the reliability of the model, experimental trends of calcium and sodium ion concentrations in the brine were compared with model predictions. As can be seen in Figure 10-b, concentration trends are well predicted by the model. A maximum discrepancy of ~4% was obtained for the sodium concentration, while 3% for the calcium concentration.

4.1.1 Hydroxyl and chloride ions transmembrane fluxes

The heart of the CrIEM reactor is the anion exchange membrane (AEM) employed to accomplish a selective passage of only anions from a solution to an adjacent one. Therefore, attention was placed to the modelling of the hydroxyl and chloride ions fluxes across the membrane. Figure 11

presents a comparison between the model and experimental total transmembrane fluxes of hydroxyl ions for case 1 of Test 1 and Test 2.

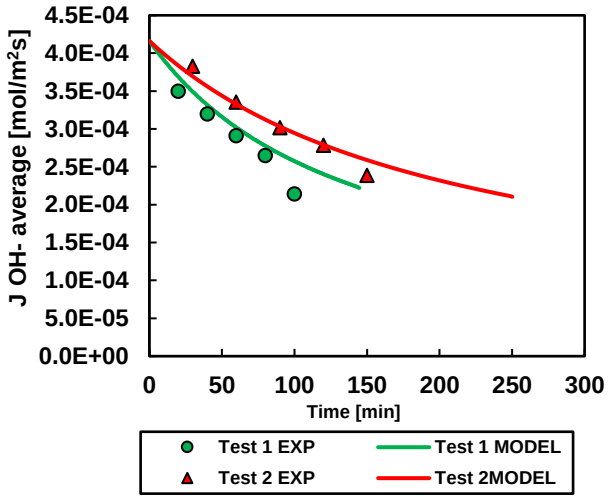

Figure 8.Comparison between model predictions and experimental results for the transmembrane fluxes of hydroxyl ions over time for Test 1 and Test 2.

As can be seen in Figure , model predictions exhibit similar trends to the experimental ones, although they underestimate hydroxyl ion fluxes, showing a maximum discrepancy between model predictions and experimental results of ~17%.

As discussed in section 3.1.2, the anionic transmembrane flux consists of two contributions: the diffusion and migrative one. Figure reports the total, the migrative and the diffusive transmembrane flux trends of hydroxyl and chloride ions for case 1 of Test 1 at the beginning (t=0 min) and at the end (t=170 min) of the test predicted by the model.

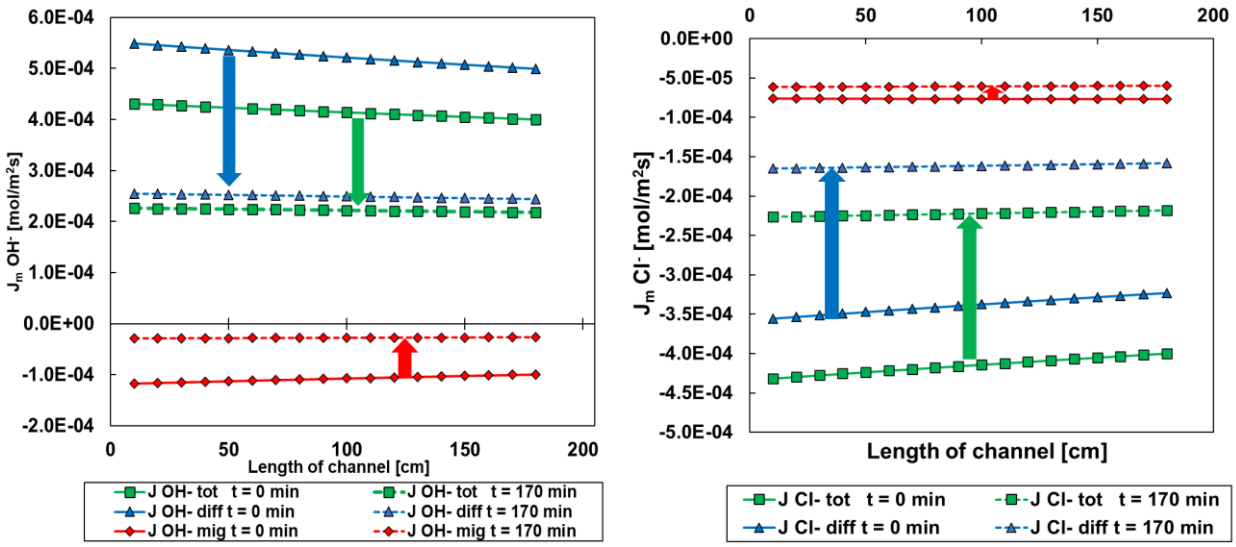

a) **b)**

Figure 9.Trend of the total transmembrane, diffusive and migration fluxes of hydroxyl and chloride ions along the channel at the beginning and end of the test predicted by the model for Test 1 ;a) hydroxyl ion flux and b) chloride ion flux.

From Figures 12 a and b it can be observed that: (i) all fluxes decrease over time due to the permeation of Cl^- ions through the membrane, causing a reduction of the driving force of the process; (ii) the diffusive flux is the main contribution to the total ion fluxes prevailing over the migrative one; (iii) diffusive fluxes and migrative fluxes have opposite direction in the case of OH^- ions, while they have the same direction in the case of Cl^- ions. In fact, the migrative contributions move ions from a region at a lower potential to the one at a higher potential, i.e. from the brine to the alkaline solution for both OH^- and Cl^- ions. Meanwhile, OH^- and Cl^- ions have opposite diffusive fluxes due to the sign of their driving force, i.e. concentration gradient between brine and alkaline solutions (Eq. (12)).

4.2 Feed and Bleed configuration

The above discussed comparison between model predictions and experimental results proved the reliability of the developed model to simulate the functioning of a CrIEM reactor in a batch configuration. On the other hand, feed & bleed arrangements can allow a continuous application of a CrIEM system to produce magnesium hydroxide particles from brines. To this aim, the developed model was adequately extended for the simulation of this new configuration, see

Section 3.2 for further details. In this case, model predictions were compared with literature experimental data presented by La Corte et al. [20]. Two cases were analysed: Test 3 and Test 6 (see Table 2 in [20]). Test 3 concerned the treatment of a real industrial brine produced in coal mining activities, while Test 6 was referred to the use of real seawater withdrawn from the northern coast of Sicily. Table 3 summarises the operating conditions of the two above mentioned cases.

Table 3. Initial composition of the main ions of brine and alkaline solutions and operative conditions adopted in the feed & bleed configuration, values are taken from [20].

Tests	Ions concentration in the Brine solution [g/l]				Concentration in the alkaline suspension [g/l]	Flow-Rate in the CrIEM [ml/min]		Initial Volume [l]		Feed & Bleed flow rate [ml/min]
	Na^+	Ca^{2+}	Mg^{2+}	Cl^-	$Ca(OH)_2$	Brine	Alkaline	Brine	Alkaline	
3	10.7	1.12	1.13	21.8	10.0	160	160	2.00	5.00	9.00
6	11.7	0.49	1.47	23.2	10.0	160	160	2.00	5.00	5.00

In Table 3, Cl^- ions concentrations were obtained considering chloride salts of Na, Ca and Mg ions. Each test was characterized by two main steps: (i) start-up step, and (ii) feed & bleed one. During the start-up step the CrIEM worked in a batch mode until reaching a desired magnesium conversion value. After that, the CrIEM was switched to a feed & bleed configuration, as explained in Section 3.2. At this point, a fresh alkaline solution was used. Moreover, during the feed & bleed operation brine samples were taken at constant time intervals. The predicted and experimental pH trends are shown in Figure 13 along with the magnesium conversion for Test 3. Sampling intervals, labelled as S1, S2, S3 and S4, are also reported.

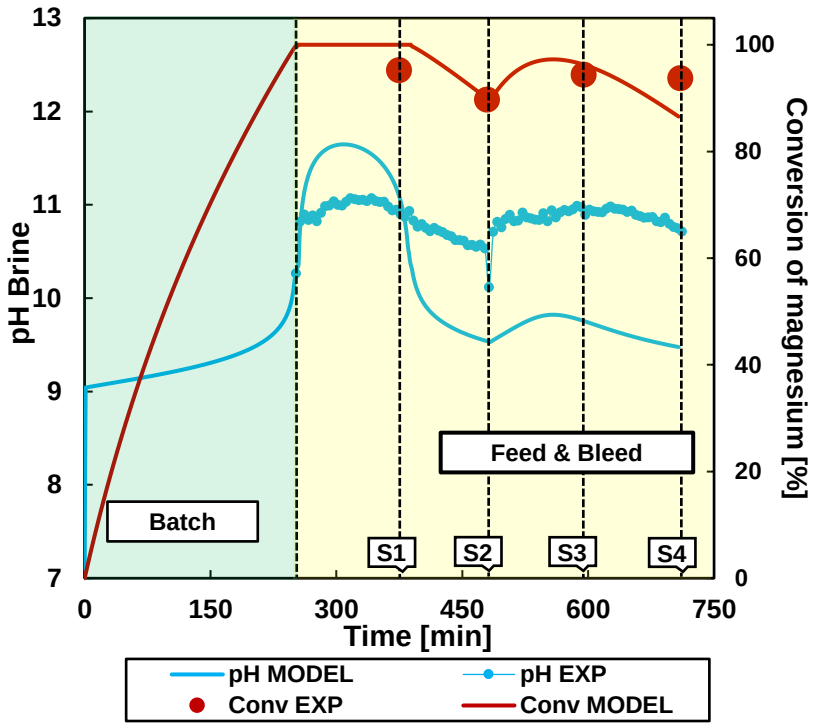

Figure 10. Comparison between model predictions and experimental results for: brine pH trends (dashed line and solid line) and magnesium conversion trend (dotted line and circle symbol) for Test 3. Labels S1,S2,S3 and S4 indicate sampling intervals. Experimental data are taken from [20].

In Figure 13 it is possible to observe that the predicted pH trend was always lower than the experimental one, with exception to the starting phase of the feed & bleed configuration. In this case the predicted pH increased to a value of ~11.5 and then decreased to ~10.8 at the first brine sampling. This is due to the fact that the model does not consider the co-precipitation of calcium as $Ca(OH)_2$ crystals, that occurs during the experiments. In fact, $Ca(OH)_2$ starts precipitating at pH values above 11, thus maintaining the solution pH between 10.8-11, as reported in La Corte et al [20]. Computed magnesium conversions were also compared with experimental values (red dots in Figure 13). A very good agreement was found, being the highest discrepancy ~5%. During the feed & bleed operation, the alkaline solution was also replaced at sampling S2. As a consequence, both the pH and the magnesium conversion increased due to higher OH- fluxes. After, they decreased due to the accumulation of Cl- ions in the alkaline solution. The model predicted well the experimental behaviour as shown in Figure 13.

The pH trend and the magnesium conversion predictions over time were also compared with experimental results of Test 6, as shown in Figure 14. In this case, the alkaline solution was replaced at each sampling.

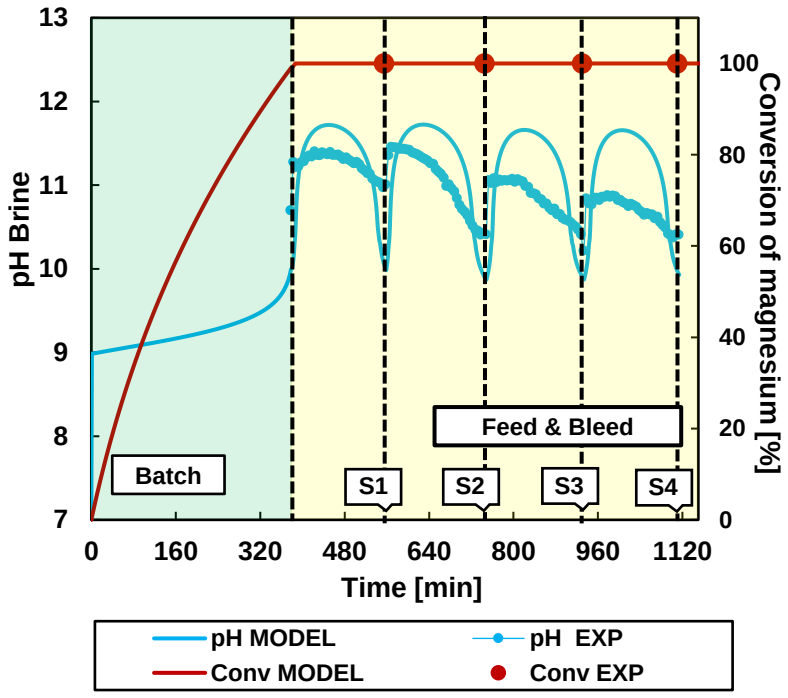

Figure 11. Comparison between model predictions and experimental results for: brine pH trends (dashed line and solid line) and magnesium conversion trend (dotted line and circle symbol) for Test 6. Labels S1,S2,S3 and S4 indicate sampling intervals. Experimental data are taken from [20].

As can been seen in Figure 14, again a satisfactory agreement between model predictions and experimental results is obtained. Magnesium conversions are better predicted than the pH trend. The reason for the higher variation of the pH is the same as the one discussed for the results of Test 3.

5 Conclusions

A novel mathematical model has been formulated for the simulation of a promising membrane-based crystallizer called “CrIEM”: a technology successfully employed for the recovery of magnesium from industrial and natural brines. The CrIEM was studied as a dialyzer based on the Donnan Dialysis theory. One dimensional differential spatial equations and time dependent equations were solved adopting a discrete finite difference method. An original algorithm was also developed to couple the phenomena occurring in the CrIEM reactor and in the two tanks containing the two reacting solutions. The developed model was successfully validated for the system in (i) batch and (ii) feed & bleed configurations. In particular, an ad-hoc experimental campaign was carried out at the Brine Excellence Center (BEC) at the University of Palermo to collect experimental data regarding the batch configuration. Literature available data were employed for the feed & bleed arrangement. A satisfactory agreement between model predictions and experimental data was achieved in all cases. Magnesium conversion was well predicted exhibiting discrepancies lower than 5%. Moreover, ions concentrations in the brine channel, hydroxyl fluxes through the membrane and pH trends were well described by the model. Results proved the reliability of the developed model to simulate CrIEM systems in a wide range of operating conditions, thus being a valuable tool for the design of this attractive membrane technology.

Acknowledgements

This work was funded by the ZERO BRINE project (ZERO BRINE – Industrial Desalination – Resource Recovery – Circular Economy) - Horizon 2020 programme, Project Number: 730390: www.zerobrine.eu.

The authors would further like to thank Fujifilm for supplying the AEM membranes necessary for the CrIEM experimental set-up.

Acronyms and nomenclature

List of acronyms

AEM	Anion exchange membrane
BEC	Brine Excellence Center
CrIEM	Crystallizer with Ion exchange membrane
EU	European Union

IC	Ionic chromatography
PE	Polyethylene

Nomenclature

A_m	Membrane area [m^2]
β	Hydration number of ion [-]
C	Concentration of ion [mol/m^3]
D	Diffusion coefficient of ion [m^2/s]
δ	Width of membrane [m]
ΔC	Concentration gradient of the between the two surfaces of the membrane [mol/m^3]
Δψ	Electric potential gradient within the membrane [V].
Δπ	Osmotic pressure gradient between the two channels [Pa]
Δx	Spatial discretization size [m]
F	Faraday constant [C/mol]
$F^{1,3}$	Flow rate of the alkaline/brine solution [m^3/s]
K	Mass transport coefficient in the brine/alkaline channel [m/s],
P_{os}	Water permeability of the membrane [m3/(Pa m2 s)]
R	Universal gas constant [J/molK]
ρ	Density of alkaline/brine solution [Kg/m^3]
t	Time [s]
T	Absolute temperature [K]
V	Volume of solution in alkaline/brine tank [m^3]
z	Chemical valence of ion [-]

Subscripts

i	ion species in the brine solution
IN	Inlet
j	ion species in the alkaline solution
OUT	Outlet

Apexes

1	Alkaline channel side
3	Brine channel side
calc	Calculated
Dyn	Dynamic
m	Membrane

References

[1] European Commission, Study on the review of the list of Critical Raw Materials - Final Report, 2020. https://doi.org/10.2873/11619.

[2] https://www.statista.com/statistics/569515/primary-magnesium-production-worldwide/, (n.d.).

[3] A. Cipollina, M. Bevacqua, P. Dolcimascolo, A. Tamburini, A. Brucato, H. Glade, L. Buether, G. Micale, Reactive crystallisation process for magnesium recovery from concentrated brines, Desalin. Water Treat. 55 (2015) 2377–2388. https://doi.org/10.1080/19443994.2014.947771.

[4] S. Wietlisbach, Latest developments and outlook for magnesium minerals and chemicals: Minerals production, market consumption drivers, new projects and forecast, 7th June 2018 Ind. Miner. Congr. Barcelona. (2018).

[5] A. Cipollina, A. Misseri, G.D.A. Staiti, A. Galia, G. Micale, O. Scialdone, Integrated production of fresh water, sea salt and magnesium from sea water, Desalin. Water Treat. 49 (2012) 390–403. https://doi.org/10.1080/19443994.2012.699340.

[6] N. Ghaffour, J. Bundschuh, H. Mahmoudi, M.F.A. Goosen, Renewable energy-driven desalination technologies: A comprehensive review on challenges and potential applications of integrated systems, Desalination. 356 (2015) 94–114. https://doi.org/10.1016/j.desal.2014.10.024.

[7] R. Zettler, A.C. Blanco, J.F. Dos Santos, S. Marya, The Effect of Process Parameters and Tool Geometry on Thermal Field Development and Weld Formation in Friction Stir Welding of the Alloys AZ31 and AZ61, Essent. Readings Magnes. Technol. 9781118858 (2014) 529–543. https://doi.org/10.1002/9781118859803.ch86.

[8] T. Peters, D. Pintó, Seawater intake and pre-treatment/brine discharge - environmental issues, Desalination. 221 (2008) 576–584. https://doi.org/10.1016/j.desal.2007.04.066.

[9] M. Latorre, Environmental impact of brine disposal on Posidonia seagrasses, Desalination. 182 (2005) 517–524. https://doi.org/10.1016/j.desal.2005.02.039.

[10] S. Lattemann, Development of an enviromental impact assessment and decision support system for seawater desalination plants, 2010.

[11] I.S. Al-mutaz, P.O. Box, Jeddah III Duba II Al-Wajh II Al-Jubail II Al-Khobar II 27 . Al-Khafji II C) Projects, Construction. 64 (1987) 97–110.

[12] I.S. Al Mutaz, K.M. Wagialia, Production of magnesium from desalination brines, Resour. Conserv. Recycl. 3 (1990) 231–239. https://doi.org/10.1016/0921-3449(90)90020-5.

[13] M. Turek, W. Gnot, Precipitation of Magnesium Hydroxide from Brine, Ind. Eng. Chem.

Res. 34 (1995) 244–250. https://doi.org/10.1021/ie00040a025.

[14] M. Turek, P. Dydo, R. Klimek, Salt production from coal-mine brine in ED-evaporation-crystallization system, Desalination. 184 (2005) 439–446. https://doi.org/10.1016/j.desal.2005.03.047.

[15] S.W. Lee, J.H. Lim, Recovery of Magnesium Oxide and Magnesium Hydroxide from the Waste Bittren, Adv. Mater. Res. 26–28 (2007) 1019–1022. https://doi.org/10.4028/www.scientific.net/amr.26-28.1019.

[16] C. Henrist, J.P. Mathieu, C. Vogels, A. Rulmont, R. Cloots, Morphological study of magnesium hydroxide nanoparticles precipitated in dilute aqueous solution, J. Cryst. Growth. 249 (2003) 321–330. https://doi.org/10.1016/S0022-0248(02)02068-7.

[17] M.H. Gong, M. Johns, E. Fridjonsson, P. Heckley, Gong: Magnesium Recovery from Desalination Brine, (2018) 49–54.

[18] M. Micari, A. Cipollina, A. Tamburini, M. Moser, V. Bertsch, G. Micale, Combined membrane and thermal desalination processes for the treatment of ion exchange resins spent brine, Appl. Energy. 254 (2019) 113699. https://doi.org/10.1016/j.apenergy.2019.113699.

[19] M. Micari, A. Cipollina, A. Tamburini, M. Moser, V. Bertsch, G. Micale, Techno-economic analysis of integrated processes for the treatment and valorisation of neutral coal mine effluents, J. Clean. Prod. 270 (2020) 122472. https://doi.org/10.1016/j.jclepro.2020.122472.

[20] D. La Corte, F. Vassallo, A. Cipollina, M. Turek, A. Tamburini, G. Micale, A novel ionic exchange membrane crystallizer to recover magnesium hydroxide from seawater and industrial brines, Membranes (Basel). 10 (2020) 1–14. https://doi.org/10.3390/membranes10110303.

[21] A.. B.M. Cipollina, A.; Micale, G.; Brucato, A.; Tamburini, Reattore e procedimento per effettuare reazioni selettive, IT Patent 102015000042831, 6, August, 2015.

[22] K. Scott, Recovery of Salts, Acids and Bases, Handb. Ind. Membr. (1995) 691–722. https://doi.org/10.1016/b978-185617233-2/50019-2.

[23] M. La Cerva, L. Gurreri, A. Cipollina, A. Tamburini, M. Ciofalo, G. Micale, Modelling and cost analysis of hybrid systems for seawater desalination: Electromembrane pre-treatments for Reverse Osmosis, Desalination. 467 (2019) 175–195. https://doi.org/10.1016/j.desal.2019.06.010.

[24] R.C. Ropp, Group 16 (O, S, Se, Te) Alkaline Earth Compounds, 2013. https://doi.org/10.1016/b978-0-444-59550-8.00003-x.

[25] P. Bajpai, Introductory Chemistry Reviews, Biermann's Handb. Pulp Pap. (2018) 401–426. https://doi.org/10.1016/b978-0-12-814238-7.00020-9.

[26] K.S. Spiegler, Polarization at ion exchange membrane-solution interfaces, Desalination. 9 (1971) 367–385. https://doi.org/10.1016/0011-9164(71)80005-X.

[27] T. Xu, Ion exchange membranes: State of their development and perspective, J. Memb. Sci. 263 (2005) 1–29. https://doi.org/10.1016/j.memsci.2005.05.002.

[28] P. Szczepański, G. Szczepańska, Donnan dialysis − A new predictive model for non−steady state transport, J. Memb. Sci. 525 (2017) 277–289. https://doi.org/10.1016/j.memsci.2016.11.017.

[29] H. Strathmann, Ion-Exchange Membrane Separation Processes, Balaban Desalination Pubblications, 2016. https://doi.org/10.1016/j.seppur.2004.05.007.

[30] M.G. Marino, J.P. Melchior, A. Wohlfarth, K.D. Kreuer, Hydroxide, halide and water transport in a model anion exchange membrane, J. Memb. Sci. 464 (2014) 61–71. https://doi.org/10.1016/j.memsci.2014.04.003.

[31] S. Ring, D. Hasson, H. Shemer, R. Semiat, Simple modeling of Donnan separation processes, J. Memb. Sci. 476 (2015) 348–355. https://doi.org/10.1016/j.memsci.2014.12.001.

[32] D. Hasson, A. Beck, F. Fingerman, C. Tachman, H. Shemer, R. Semiat, Simple model for characterizing a Donnan dialysis process, Ind. Eng. Chem. Res. 53 (2014) 6094–6102. https://doi.org/10.1021/ie404291q.

[33] R. Gueccia, S. Randazzo, D. Chillura Martino, A. Cipollina, G. Micale, Experimental investigation and modeling of diffusion dialysis for HCl recovery from waste pickling solution, J. Environ. Manage. 235 (2019) 202–212. https://doi.org/10.1016/j.jenvman.2019.01.028.

[34] D. Lundberg, A.S. Ullström, P. D'Angelo, I. Persson, A structural study of the hydrated and the dimethylsulfoxide, N,N′-dimethylpropyleneurea, and N,N-dimethylthioformamide solvated iron(II) and iron(III) ions in solution and solid state, Inorganica Chim. Acta. 360 (2007) 1809–1818. https://doi.org/10.1016/j.ica.2006.09.014.

[35] E.J. Lam, M.N. Alvarez, M.E. Galvez, E.B. Alvarez, A model for calculating the density of

aqueous multicomponent electrolyte solutions, J. Chil. Chem. Soc. 53 (2008) 1404–1409. https://doi.org/10.4067/S0717-97072008000100015.